

# Genome edited colorectal cancer organoid models reveal distinct microRNA activity patterns across different mutation profiles

Jonathan W. Villanueva<sup>1</sup>, Lawrence Kwong<sup>1</sup>, Teng Han<sup>2</sup>, Salvador Alonso Martinez<sup>2</sup>, Fong Cheng Pan<sup>3</sup>, Michael T. Shanahan<sup>1</sup>, Matt Kanke<sup>1</sup>, Shuibing Chen<sup>3</sup>, Lukas E. Dow<sup>2</sup>, Charles G. Danko<sup>1,4\*</sup> and Praveen Sethupathy<sup>1\*</sup>

<sup>1</sup>*Department of Biomedical Sciences, College of Veterinary Medicine, Cornell University, Ithaca, NY, 14853, USA*

<sup>2</sup>*Sandra and Edward Meyer Cancer Center, Department of Medicine, Weill Cornell Medicine, Cornell University, New York, NY, 10065, USA*

<sup>3</sup>*Department of Surgery, Weill Cornell Medicine, 1300 York Ave, New York, NY, 10065, USA*

<sup>4</sup>*Baker Institute for Animal Health, College of Veterinary Medicine, Cornell University, Ithaca, NY 14853, USA*

\* *Corresponding author*

Correspondence: [pr46@cornell.edu](mailto:pr46@cornell.edu), [cgd24@cornell.edu](mailto:cgd24@cornell.edu)

## Abstract

Somatic mutations drive colorectal cancer (CRC) by disrupting gene regulatory mechanisms. Distinct combinations of mutations can result in unique changes to regulatory mechanisms leading to variability in the efficacy of therapeutics. MicroRNAs are important regulators of gene expression, and their activity can be altered by oncogenic mutations. However, it is unknown how distinct combinations of CRC-risk mutations differentially affect microRNAs. Here, using genetically-modified mouse intestinal organoid (enteroid) models, we identify ten different modules of microRNA expression patterns across distinct combinations of mutations common in CRC. We also show that miR-24-3p, which is aberrant in genetically-modified mouse enteroids and human colonoids irrespective of mutational context, is a master regulator of gene expression in CRC. In follow-up experiments, we also demonstrate that miR-24 promotes CRC cell survival. These findings offer insight into the mechanisms that drive inter-tumor heterogeneity and highlight candidate microRNA therapeutic targets for the advancement of precision medicine for CRC.

## Introduction

Colorectal cancer (CRC) is estimated to be the third most diagnosed cancer and the second leading cause of cancer-related death worldwide<sup>1</sup>. A major challenge in treating CRC patients is that molecular differences across patients' tumors, or inter-tumor heterogeneity, can lead to highly variable patient outcomes<sup>2-4</sup>. Recent advances in the understanding of CRC inter-tumor heterogeneity have led to substantial improvements in the therapeutic strategies utilized to treat CRC patients<sup>4-6</sup>. One notable example is how tumors are screened for *KRAS*, *NRAS*, and *BRAF* mutations to determine eligibility for anti-EGFR monoclonal antibody treatment<sup>5,6</sup>. This example represents only the beginning of the promise of personalized approaches for CRC, and strongly

motivates the goal of understanding how different combinations of somatic mutations in key oncogenes and tumor suppressors promote molecular variability across tumors.

Mutation status plays a key role in inter-tumor heterogeneity through genotype-specific alterations of gene regulatory mechanisms that control tumor growth and development<sup>7-9</sup>. Unique combinations of driver mutations have been shown to lead to novel cancer phenotypes, including resistance to WNT inhibitors in intestinal mouse models of CRC<sup>10-12</sup>. However, most studies that investigate the effects of genetic alterations on gene regulatory mechanisms focus on the effects of individual mutations<sup>13-16</sup>. Therefore, there is a critical need to investigate how combinations of distinct CRC mutations alter regulatory mechanisms and drive novel cancer phenotypes.

MicroRNAs (miRNAs) are small, ~22 nt non-coding RNAs that canonically function as post-transcriptional, negative regulators of gene expression. It has been well documented that abnormal activity of certain miRNAs can initiate and/or exacerbate disease phenotypes, including cancer<sup>17-19</sup>. Although there remain some challenges to miRNA-based therapeutics (as with many other classes of molecular therapy), several have shown promise in pre-clinical models of cancer (such as miR-10b and breast cancer<sup>20</sup>) and some have been nominated for clinical trials<sup>21</sup> and/or are currently in different phases of clinical trials<sup>22</sup>. Numerous studies have demonstrated that miRNAs are significantly altered in CRC tissues<sup>23-25</sup>. While miRNA-based therapies have been proposed for CRC<sup>26</sup>, to our knowledge none are currently in clinical trials. Moreover, importantly, it remains unknown how different combinations of driver mutations affect miRNA profiles and how this promotes unique tumor phenotypes.

A major challenge in evaluating how combinations of mutations affect miRNA profiles has been a lack of appropriate cellular models. Primary tumors harbor tens to hundreds of non-silent mutations and are therefore not ideal for evaluating the effects of specific genotypes<sup>27</sup>. Additionally, primary tumors are highly heterogenous and this limits our ability to assess mutation-specific miRNA alterations in the epithelium where CRC tumors form. CRC cell models also have several mutations<sup>28</sup> and are limited in their ability to recapitulate the biology of the intestinal epithelium. To address these limitations, researchers have developed genetically modified organoid models that mimic the physiology of the intestinal epithelium. Using gene editing tools (CRISPR/Cas9, Cre), specific combinations of mutations can be induced to evaluate their impact on cell behavior and/or sensitivity to therapeutics<sup>12,29</sup>. To our knowledge, these state-of-the-art intestinal model systems have not yet been used to study mutation-specific changes to miRNA profiles.

To address the important knowledge gaps mentioned above, we leverage genetically modified mouse small intestinal epithelial organoids (termed enteroids) to characterize how miRNA profiles change in response to different combinations of CRC driver mutations. Using small RNA-seq, we define different patterns of miRNA expression across various genotypes, which also reveals the dominant role of Tgf- $\beta$  signaling in the regulation of predicted tumor suppressor miRNA, miR-375-3p. By leveraging this mouse enteroid data, in conjunction with small RNA-seq data from human primary colon tumor data from The Cancer Genome Atlas (TCGA)<sup>28</sup> and RT-qPCR data from genetically modified human colonic epithelial organoids (termed colonoids), we find that miR-24-3p is up-regulated across all mutational contexts and is a candidate master regulator of gene expression in CRC. Additional studies in multiple cell modes demonstrate that miR-24-3p inhibition results in a significant decrease in cell viability by inducing apoptosis. Finally, we perform integrative analysis of RNA-seq and chromatin run-on sequencing (ChRO-seq)<sup>30</sup> to identify *HMOX1* and *PRSS8* as genes subject to strong post-transcriptional regulation by miR-24-3p in CRC. Overall, this study offers, to our knowledge, the first genome-scale characterization of miRNA patterns across distinct combinations of CRC driver mutations,

provides new insight into the molecular mechanisms that drive inter-tumor heterogeneity, and defines candidate miRNA targets for future therapeutic development in CRC irrespective of mutational context.

## Results

### *Genetically modified enteroids exhibit mutation-specific variation in miRNA expression*

To characterize the effect of genotype on miRNA expression we performed small RNA-seq on mouse enteroids that harbor different combinations of CRC mutations. We focused on mutations in genes that are in signaling pathways commonly dysregulated in CRC according to The Cancer Genome Atlas (TCGA) (**Fig 1A, Table S1**)<sup>2,12,31-33</sup>: Wnt (*Ctnnb1*, *Apc*, and *Rspo3*; 181/195 tumors in TCGA contain at least one mutation affecting this pathway), p53 (*p53*; 120/195 tumors in TCGA contain at least one mutation affecting this pathway), Mapk (*Kras*; 122/195 tumors in TCGA contain at least one mutation affecting this pathway), and Tgf- $\beta$  (*Smad4*; 70/195 tumors in TCGA contain at least one mutation affecting this pathway). Using miRquant 2.0, a small RNA-seq analysis tool<sup>34</sup>, we profiled miRNAs across enteroids with 9 different genotypes. Principal component analysis (PCA) revealed that miRNA profiles stratify enteroid samples by mutational combinations (**Fig 1B**). Moreover, the majority of mutant enteroids are clearly separated from wild-type (WT) in the PCA plot. The analysis also showed that *Rspo3* mutant enteroids are most similar to WT controls, which is in line with previous morphological and RNA-seq comparisons<sup>33</sup>. Therefore, *Rspo3* mutants were not incorporated into the downstream analyses.

Next we sought to define miRNA expression patterns across the 6 genotypes for which we have at least two biological replicates. Specifically, we performed a likelihood ratio test using DESeq2, which revealed 151 miRNAs with significant expression variation across genotypes (p-adj<0.05, baseMean>500). We grouped these miRNAs into 10 distinct expression profiles, or “modules”, using DEGREport<sup>35</sup> (**Fig 1C, S1A**). Group I

(**Fig 1D**) is composed of miRNAs that exhibit a comparable increase in expression across all genotypes relative to WT, hereafter referred to as mutation-independent effects. One prominent example of a Group I miRNA is miR-146a-5p<sup>36,37</sup>, which functions as an oncogenic miRNA in CRC. All remaining modules exhibited non-uniform effects on miRNA expression; that is, larger changes in specific genotypes compared to others (mutation-dependent effects).

In certain modules of mutation-dependent miRNAs, we observed that specific combinations of mutations resulted in a combined effect (synergistic or additive) on expression. Group C (**Fig 1E**) is an example of such a module. MiRNAs in this group are elevated in mouse enteroids with either *Kras/Rspo3/p53* (KRP) or *Kras/Rspo3/Smad4* (KRS) mutant genotypes and most dramatically increased in *Kras/Rspo3/p53/Smad4* (KRPS) mutant enteroids. This group, which includes established oncogenic miRNAs such as miR-21-5p<sup>38,39</sup> and miR-23a-3p<sup>40,41</sup>, highlights a potential miRNA mechanism by which the combination of *KRAS*, *P53*, and *SMAD4* mutations may promote severe patient outcomes<sup>42,43</sup>.

We also identified modules with miRNAs that exhibit the largest expression change in enteroids with the lowest number of mutations. One such example is Group F (**Fig 1F**), in which miRNAs change the most relative to WT in *Apc* (A), *Ctnnb1* (B), and KRP mutant enteroids. This group includes tumor suppressor miRNAs such as miR-30a-5p<sup>44,45</sup> and miR-141-3p<sup>46,47</sup>. Although KRPS mutant enteroids harbor the largest number of mutations, the miRNAs in Group F exhibit only a slight elevation in this genotype. This data supports the conclusion that changes in oncogenic and tumor suppressor miRNA expression are driven by specific mutational combinations, and not just total mutational burden.

### ***Modification of Tgf-β/Smad4 signaling is sufficient to drive miR-375-3p expression in mouse enteroids***

We next sought to investigate how mutations in one specific pathway can play a prominent role in the expression of miRNAs. We turned to modules in which the most significant changes in miRNA expression occur in enteroids harboring a *Smad4* mutation. Group D consists of miRNAs that exhibit the highest

expression in the enteroids with KRS and KRPS genotypes (**Fig 2A**), whereas Group B consists of miRNAs with the lowest expression in these two genotypes (**Fig 2B**). The latter includes miR-375-3p (**Fig 2C**), which has been reported to function as a tumor suppressor in several different cancer types<sup>48-50</sup>.

The only difference between KRP and KRPS is the presence of the *Smad4* knockout mutation. Our findings in **Fig 2C** suggest that the loss of *Smad4* has a prominent suppressive effect on miR-375-3p, which directly motivates the hypothesis that Tgf- $\beta$  signaling is sufficient to increase miR-375-3p expression in mouse enteroids. To test this hypothesis, enteroids from WT B62J mice were treated with 0, 0.5, or 1 ng/mL Tgf- $\beta$  for 3 days and changes in miR-375-3p were measured by RT-qPCR. Tgf- $\beta$  treatment led to a significant increase in miR-375-3p compared to control (**Fig 2D**). These results confirm our hypothesis that the candidate tumor suppressor miRNA, miR-375-3p, from Group B is most strongly driven by changes in Tgf- $\beta$ /Smad4 signaling in the intestine.

### ***Identification of five candidate miRNA master regulators in genetically modified mouse enteroid models of CRC***

We next investigated miRNAs that are consistently up- or down-regulated across all mutational combinations. These miRNAs may regulate CRC phenotypes irrespective of mutational context and therefore could represent attractive candidates for generalized therapy. We identified 28 miRNAs that are significantly differentially expressed in each mutant enteroid genotype relative to WT control (**Fig 3A, B**; DESeq2<sup>51</sup> baseMean >500, >1.5x fold change in the same direction across all 5 comparisons, p-value < 0.05 and p-adj < 0.2 in at least 4 out of 5 comparisons)

We next performed RNA-seq in the same mutant enteroid models (**Table S2, Fig S2**) to evaluate changes in expression of the genes that are predicted targets of the most altered miRNAs. Of the 28 miRNAs that exhibit changes across all mutational contexts, we removed isomiRs, inactive strand ('star strand') miRNAs, and miRNAs that were not conserved in >2 out of the 5 species considered by our previously

described statistical simulation tool, miRhub<sup>52</sup> (**Fig 3C**). This left 7 upregulated and 11 downregulated miRNAs for a miRNA target site enrichment analysis by miRhub, which identified 2 upregulated miRNAs with a significant enrichment (p-value<0.05 in at least 3 out of 5 WT vs mutant enteroid comparisons) of predicted gene targets in the lists of downregulated genes and 3 downregulated miRNAs with a significant enrichment of predicted gene targets in the lists of upregulated genes (**Fig 3D**; p-value<0.05 in at least 3 out of 5 WT vs mutant enteroid comparisons). These 5 miRNAs consist of two paralogs of miR-24-3p, two paralogs of miR-194-5p, and miR-141-3p (**Fig 3E**), each of which represent candidate master regulators of gene expression across various mutational contexts and may provide insight into the molecular underpinnings of the pathways central to CRC phenotypes.

### ***miR-24-3p is a candidate master regulator of gene expression and cancer phenotypes in the human colonic epithelium***

To place our mouse enteroid studies in a more clinically relevant context, we downloaded small RNA- and RNA-seq data from human primary colon adenocarcinoma and non-tumor tissue analyzed by TCGA<sup>2</sup>. Removing miRNAs with average expression under 1000 reads per million mapped to miRNAs (RPMMM) in either the tumor or non-tumor condition left 65 miRNAs with a significant change of expression in the tumor compared to non-tumor control (**Fig 4A**; fold change >1.5x, p-adj<0.05). Next, we identified 3190 differentially expressed genes (DESeq2; average expression > 1000 normalized counts, >1.5x fold change, p-adj<0.05). Of the 65 miRNAs that are altered in human CRC tumors, 17 exhibit a significant enrichment of predicted targets among genes that change significantly in the opposite direction of the miRNA (miRhub p-value<0.05; **Fig 4B**). To account for the genetic cofounders that emerge when comparing primary tumors of one patient to non-tumor tissue from another patient, we also performed a differential miRNA expression analysis between matched tissues (n=8). Of the 17 miRNAs identified above, 15 are still significantly altered when the analysis is restricted to matched samples (**Fig 4C**).



Of these 15 miRNAs that are candidate master regulators of gene expression in human CRC, only miR-24-3p was also identified as a candidate master regulator of gene expression in the mouse enteroid analyses (**Fig 4D**). We next assessed changes in miR-24-3p expression across 23 different tumor types relative to their corresponding non-tumor tissue. Of these, rectal adenocarcinoma (READ) and colon adenocarcinoma (COAD) had the highest upregulation of miR-24-3p (**Fig 4E**), indicating that miR-24-3p upregulation is strongest in CRC.

Given the upregulation of miR-24-3p we observed in our mouse enteroid models, we hypothesized that upregulation of miR-24-3p in the heterogeneous TCGA colon tumors is driven, at least in part, by changes in the colonic epithelium. To evaluate this hypothesis in a human system, we examined miR-24-3p in genetically modified colonic organoids, termed colonoids, harboring mutations in genes commonly mutated in CRC (**Fig 4F**). It has been previously illustrated that these colonoid models are representative of the colonic epithelium and the induction of specific mutations has also been confirmed<sup>29</sup>. Using RT-qPCR, we found a significant elevation in miR-24-3p expression across all six mutant colonoids compared to iGFP controls (**Fig 4G**). Thus, we conclude that the upregulation of miR-24-3p in CRC is driven, at least in part, in the colonic epithelium.

### ***Reduction of miR-24-3p increases apoptosis in HCT116 cells***

We hypothesized that miR-24-3p promotes colon tumor phenotypes. To evaluate this hypothesis, we performed loss-of-function studies in HCT116 cells, which is derived from a microsatellite instable human colon tumor with mutations in *CTNNB1*, *KRAS*, and *TGFBR3*. Specifically, we treated HCT116 cells with a miR-24-3p locked nucleic acid (LNA) inhibitor, which led to significantly reduced detection of miR-24-3p (**Fig 5A**). HCT116 cultures treated with a miR-24-3p inhibitor exhibited a significant reduction in cell number compared to mock and scramble controls (**Fig 5B**). We also observed a significant reduction in the number of metabolically active, viable cells (**Fig 5C**). These results support our hypothesis that miR-24-3p promotes cell viability in CRC.

Next we asked whether the change in cell viability was caused by differences in the rate of cell proliferation, cell death, or both. To evaluate changes in proliferation, we performed an EdU incorporation assay. Our analysis showed a significant decrease in the number of DAPI+ cells (**Fig S3A**) but did not identify a significant change in the percentage of EdU+ cells after treatment with miR-24-3p inhibitor relative to mock or scramble controls (**Fig 5D**). To evaluate changes in apoptosis, we performed a TUNEL assay. HCT116 cells treated with a miR-24-3p inhibitor displayed a significant decrease in the number of DAPI+ cells (**Fig S3B**) and an increase in the percentage of TUNEL+ cells compared to mock and scramble controls (**Fig 5E**). Thus, we conclude that miR-24-3p promotes CRC cell viability at least in part through suppression of apoptosis (and not through increased proliferation).

### ***miR-24-3p inhibition decreases mouse enteroid survival and size***

To further validate the role of miR-24-3p in regulating cell survival in the intestine, we next examined the effects of miR-24-3p inhibition on the growth and viability of mouse enteroids. Jejunal crypts were isolated from WT B62J mice and cultured *ex vivo* to establish enteroids, which were treated with either a miR-24-3p LNA inhibitor or scramble control for a total of five days. Enteroid cultures treated with the miR-24-3p inhibitor exhibited significant (33%) reduction in the number of enteroids (**Fig 6A, Fig S4A**). However, enteroids treated with a miR-24-3p inhibitor did not exhibit a significant difference in enteroid size relative to those treated with the scramble control (**Fig 6B, Fig S4B**). Taken together, these results provide further support that miR-24-3p promotes cell survival of intestinal epithelial cells.

### ***HMOX1 is a direct target gene of miR-24 in the human colon context***

To identify candidate gene targets by which miR-24-3p exerts its function in CRC, we treated HCT116 cells with miR-24-3p LNA inhibitor or scramble control. After 48 hrs, we isolated RNA from these cells and

performed an RNA-seq analysis to identify genes that change in response to miR-24-3p inhibition (**Table S3**). We reasoned that direct target genes should be inversely correlated with miR-24-3p; therefore, we focused our subsequent analyses on the 222 genes that are significantly elevated (expression above 500 normalized counts in either condition,  $p\text{-adj} < 0.05$ , Fold change  $> 0$ ) in response to miR-24-3p inhibition (**Fig 7A**). Of these genes, 70 were identified as predicted miR-24-3p targets (**Fig 7B**). We performed a KEGG pathway analysis using Enrichr<sup>53-55</sup> (**Fig 7C**), which revealed that up-regulated genes with predicted miR-24-3p targets are enriched in apoptosis and ferroptosis pathways (two different forms of cell death). Notably, nine of the 70 predicted miR-24-3p target genes are also significantly downregulated (DESeq2; average expression  $> 1000$  normalized counts,  $> 1.5x$  fold change,  $p\text{-adj} < 0.05$ ) in TCGA colon tumor relative to non-tumor tissue (**Fig 7B**), including *HMOX1* and *PRSS8*, which exhibited the highest upregulation among the nine (**Fig 7D**). Moving forward, we focused on *HMOX1* and *PRSS8*, which have been shown previously to regulate cell survival in various cancer contexts<sup>56-59</sup>.

As an independent validation of the RNA-seq analysis, we performed RT-qPCR analysis for *HMOX1* and *PRSS8* using RNA from HCT116 cells treated with a miR-24-3p LNA inhibitor or scramble control. As expected, both genes exhibited a significant elevation in miR-24-3p inhibitor treated cells compared to control (**Fig 7E**). We also treated HCT116 cells with 50, 100, or 150 nM of miR-24-3p mimic or scramble control. Consistent with expectation, we observed a dose-dependent decrease in *HMOX1* and *PRSS8* expression (**Fig 7F**). These results support the model that miR-24-3p regulates *HMOX1* and *PRSS8* in CRC cells.

To determine whether miR-24-3p is indeed post-transcriptionally regulating *HMOX1* and *PRSS8* expression, as opposed to indirectly regulating the transcriptional activity of the two genes, we performed length extension chromatin run-on sequencing (leChRO-seq)<sup>30</sup> on HCT116 cells after LNA inhibitor treatment (**Table S4**). By comparing changes in *HMOX1* and *PRSS8* transcription (via leChRO-seq) to changes in steady-state gene expression (via RNA-seq) after treatment with the miR-24-3p inhibitor, we showed that neither gene is altered significantly at the transcriptional level even though both exhibit significant elevation at the mRNA level (**Fig 7F**). Together, this data supports that miR-24-3p regulates *HMOX1* and *PRSS8* in a CRC context.

## Discussion

In this study we leverage genetically modified mouse enteroids to characterize the impact of different combinations of CRC driver mutations on miRNA expression. We show that each of the genotypes investigated result in distinct miRNA profiles, with the exception of *Rspo3* (R) mutant enteroids which are comparable to wild-type (WT). The latter finding is consistent with previous studies that have shown R mutant enteroids exhibit similar RNA-seq profiles and cell morphology to WT enteroids<sup>33</sup>. We also define separate modules of miRNAs, each of which exhibits a unique pattern of expression across genotypes. We establish a publicly accessible resource, called ME-MIRAGE (<https://jwvillan.shinyapps.io/ME-MIRAGE/>), that allows users to evaluate mutation-specific relationships between miRNAs and genes. This database is a novel resource that provides information regarding the miRNA-mediated mechanisms by which combinations of somatic mutations can drive inter-tumor heterogeneity in CRC.

We highlight miR-375-3p as a mutation-dependent miRNA by showing that its expression is most strongly affected in the *Smad4*<sup>KO</sup> context. Interestingly, A and KRP enteroids also exhibit significantly reduced miR-375-3p expression compared to WT, however the magnitude of the decrease is much smaller relative to KRS and KRPS enteroids. This suggests that inhibition of miR-375-3p in CRC is strongly, but not solely, driven by changes in Tgf- $\beta$  signaling. Previous studies in colon, stomach, and liver cancers have established miR-375-3p as a tumor suppressor<sup>49,60,61</sup>. This is in line with our recent report that shows miR-375 inhibits cell proliferation and migration in fibrolamellar carcinoma<sup>48</sup> and suppresses proliferation in intestinal stem cells<sup>62</sup>. In CRC, we suggest that a miR-375-3p mimic could be a candidate therapeutic approach especially for patients with somatic mutations that inhibit Tgf- $\beta$  signaling.

31

32 To identify candidate master miRNA regulators of CRC gene expression, we identified miRNAs that are  
 33 consistently dysregulated in the same direction across TCGA CRC samples and mutant mouse enteroids relative  
 34 to controls. Following a target enrichment analysis, using miRhub, miR-24-3p was the only miRNA that met  
 35 the filtering criteria. MiR-141-3p also emerged from this analysis, but this miRNA was downregulated in mouse  
 36 and upregulated in primary human tumors from the TCGA. Species-specific functions for miRNAs have been  
 37 reported in the field and may be contributing to this discrepancy for miR-141-3p in our results<sup>63</sup>. Another  
 38 contributing factor could be that the mouse enteroids are derived from small intestinal tissue while human CRC  
 39 tumor tissue is derived from colon. Finally, the last confounding factor is that mouse enteroids are  
 40 representative of the intestinal epithelium while primary tumor samples contain a heterogeneous population of  
 41 cells.

42

43 The limited literature on the functional role of miR-24-3p in CRC offers mixed conclusions on whether  
 44 miR-24-3p is an upregulated oncogenic miRNA<sup>64,65</sup> or a downregulated tumor suppressor<sup>66,67</sup>. This is likely due  
 45 to a combination of pleiotropy in miR-24-3p function and the differences in experimental approaches across  
 46 studies. In this study, we leverage multiple cell models in addition to TCGA data to support that miR-24-3p is  
 47 an oncogenic miRNA in CRC. MiR-24-3p is located on the same pri-miRNA transcript as miR-27a-3p and  
 48 miR-23a-3p<sup>68</sup>. We found that all three miRNAs are significantly elevated in TCGA primary colon tumor tissue  
 49 and that genes downregulated in CRC are enriched for predicted targets of each of the miRNAs. MiR-27a-3p  
 50 and miR-24-3p are also significantly elevated in the majority of mutant enteroids relative to WT (miR-23a-3p  
 51 exhibits a more modest increase that does not reach significance in multiple genotypes relative to WT). This  
 52 consistent upregulation in the miR-23a/miR-24/miR-27a cluster across datasets supports the literature that miR-  
 53 24-3p is elevated in CRC. Moreover, our studies in human colonoids confirm that miR-24-3p is elevated in  
 54 response to all mutational combinations. Finally, functional studies in HCT116 cells and enteroids demonstrate

that inhibition of miR-24-3p suppresses CRC tumor cell apoptosis. Taken together, we propose that that miR-24-3p upregulation promotes cancer cell survival in CRC.

We identified multiple genes that are up-regulated due to loss of post-transcriptional suppression after inhibition of miR-24-3p, most notably *HMOX1* and *PRSS8*, which are also prominently downregulated in TCGA colon tumors. Given miR-24-3p inhibition leads to increased apoptosis, we predict that *HMOX1* and *PRSS8* function as tumor suppressors in CRC. While *PRSS8* has clearly been shown to promote apoptosis in multiple cancer contexts<sup>58,59</sup>, the role of *HMOX1* in regulating apoptosis appears to vary across tissues<sup>56,69,70</sup>. While the role of *HMOX1* in the colon remains to be thoroughly evaluated, studies show that *HMOX1* can function as a tumor suppressor in CRC by inhibiting tumor invasion<sup>71</sup> and metastasis<sup>72</sup>. Here we suggest that *HMOX1* may also function as a tumor suppressor by increasing apoptosis, which merits more detailed future investigation.

In our KEGG 2019 pathway enrichment analysis of upregulated genes after miR-24-3p inhibitor treatment we identified ferroptosis, a form of cell death induced by excessive iron-induced lipid peroxidation. Cell count and CellTiter-glo analyses of HCT116 cells treated with a miR-24-3p inhibitor and ferroptosis inhibitor, ferrostatin, revealed no partial recovery of cell number at increasing concentrations of ferrostatin (**Fig S5A,B**). One potential explanation for this data is that the poor stability of ferrostatin<sup>73</sup> prevented effective inhibition of ferroptosis. Another possibility is that miR-24-3p inhibition primed cells to undergo apoptosis, but without the proper induction of ferroptosis, we did not observe a change in cell number at higher concentrations of ferrostatin. Treating cells with cisplatin, or another platinum-based therapy like oxaliplatin which is commonly used to treat CRC patients, may be an appropriate stimulus as cisplatin has been shown to induce apoptosis and ferroptosis in HCT116 cells<sup>74</sup>. If miR-24-3p does inhibit ferroptotic cell death, then treating CRC

patients with a miR-24-3p inhibitor in conjunction with oxaliplatin may increase the efficacy of treatment and increase patient survival. We believe this idea merits further investigation.

Our results provide insight into the mechanisms by which somatic mutations alter miRNA profiles and how this can contribute to inter-tumor heterogeneity. Future studies in the field can build on our work by incorporating somatic mutations in genes that stratify established CRC subtypes<sup>75</sup> and observing changes in miRNA profiles. Additionally, we hope to characterize how combinations of somatic mutations affect pri-miRNA transcription to elucidate the transcriptional programs that contribute to changes in mature miRNA profiles. Ultimately, the identification of mutation-specific miRNAs will be important for identifying candidate miRNA therapeutics and the overall advancement of precision medicine for CRC patients.

## Experimental Procedures

**Generation of genetically modified mouse enteroids.** The proximal half of the small intestine was isolated from 5-6 week-old C57BL/6 mice for crypt isolation. Cells were plated in Matrigel and grown for 3-4 weeks. Enteroids were then dissociated and transfected using the necessary Cre/CRISPR gene editors.

A, B, AKP, BKP: Cells with *Apc*<sup>Q883\*</sup> mutation (A) and *Ctnnb1*<sup>S33F</sup> (B) were generated using CRISPR base editing as described in Schatoff et al. (2019)<sup>31</sup>. Selection for *Apc*<sup>Q883\*</sup> and *Ctnnb1*<sup>S33F</sup> mutants was performed by culturing cells in the absence of RSPO1. *Kras*<sup>G12D</sup> (K) and *Trp53*<sup>-/-</sup> (P) mutations were generated using enteroids from the conditional *LSL-Kras/p53<sup>fl/fl</sup>* mouse model, as described in Dow et al., (2015)<sup>32</sup>. Cre was introduced to enteroids by transfection. Cells with *Trp53*<sup>-/-</sup> mutation were selected for by treating cells with 10  $\mu$ M Nutlin3. To ensure *Kras*<sup>G12D</sup> mutation, cells were then cultured in the absence of EGF.

KRP, KRS, KRPS: *Kras*<sup>G12D</sup> mutations (K) were generated by using enteroids derived from the *Kras*<sup>LSL-G12D</sup> conditional model as described in Jackson et al. (2001)<sup>76</sup>. Cre was introduced to enteroids by transfection. Cells with the *Kras*<sup>LSL-G12D</sup> allele were selected for by adding 1 μmol/L gefitinib to the culturing media. Cells with *Ptpkr-Rspo3* fusion (R) were generated via CRISPR/Cas9 chromosome rearrangement as described in Han et al., (2017)<sup>33</sup>. Selection for *Ptpkr-Rspo3* mutants was done by culturing cells in the absence of RSPO1. *Trp53*<sup>-/-</sup> (P) and *Smad4*<sup>KO</sup> (S) mutations were generated using CRISPR/Cas9 and single guide RNAs (sgRNA) as described in Han et al., (2020)<sup>12</sup>. Selection for *Trp53*<sup>-/-</sup> cells was completed by adding 5 μmol/L Nutlin-3 to the culturing media. Selection for *Smad4*<sup>KO</sup> cells was completed by adding 5 ng/mL TGFβ1 to the culturing media.

**Trizol LS RNA isolation.** Cells were treated with 250 μL of cold 1X NUN Lysis Buffer (20 mM HEPES, 7.5 mM MgCl<sub>2</sub>, 0.2 mM EDTA, 0.3 M NaCl, 1 M Urea, 1% NP-40, 1mM DTT, and 50 units/mL SUPERase In RNase Inhibitor (ThermoFisher Scientific, Waltham, MA), and 1X 50X Protease Inhibitor Cocktail (Roche, Branchburg, NJ)). Lysate was vortexed vigorously for 1 minute to physically lyse cells. Samples were incubated for 30 minutes in Thermomixer C at 12°C at 1500 rpm. Chromatin was pelleted out by centrifuging samples for 12,500 xg for 30 minutes at 4°C. Supernatant containing RNA was removed from the tube and added to clean 1.5 mL centrifuge tube along with 750 μL Trizol LS (Life Technologies, 10296-010). Samples were vortexed and stored at -80°C until RNA isolation. Samples were thawed and allowed to incubate for 5 minutes. 200 μL of chloroform was added to each tube and vortexed for 20 seconds. Following a three-minute incubation, samples were centrifuged at 17,000 xg, 4°C for 5 minutes. Aqueous layer was transferred to clean 1.5 mL centrifuge tube containing 2.5 μL of GlycoBlue. 1 mL of ice cold, 100% ethanol was added to aqueous phase and samples were then vortexed. Samples were then centrifuged at 17,000 xg at 4°C for 15 minutes. Supernatant is removed and pellet is washed with 75% ice cold ethanol. Samples were vortexed and RNA was pelleted by centrifuging at 17,000 xg at 4°C for 5 minutes. Supernatant is removed and RNA pellets are allowed to dry for 10 minutes at room temperature. RNA was resuspended in 30 μL of RNase-free water.



74

75 **Small RNA library preparation and sequencing.** Total RNA was isolated using the Total RNA Purification  
 76 Kit (Norgen Biotek, Thorold, ON, Canada) according to manufacturer's instructions or Trizol LS method  
 77 described above. RNA purity and concentration was determined using the Nanodrop 2000 (Thermo Fisher  
 78 Scientific, Waltham, MA). RNA integrity was quantified using the 4200 TapeStation (Agilent Technologies,  
 79 Santa Clara, CA) or Fragment Analyzer Automated CE System (Advanced Analytical Technologies, Ankeny,  
 80 IA). Libraries were prepared at the Genome Sequencing Facility of the Greehey Children's Cancer Research  
 81 Institute (University of Texas Health Science Center, San Antonio, TX) using the CleanTag Small RNA Library  
 82 Prep kit (TriLink Biotechnologies, San Diego, CA). Libraries were then sequenced on the HiSeq2000 platform  
 83 (Illumina, San Diego, CA).

34

35 **RNA library preparation and sequencing.** Total RNA was isolated using the Total RNA Purification Kit  
 36 (Norgen Biotek, Thorold, ON, Canada) according to the manufacturer's instructions or using the Trizol LS  
 37 method described above. RNA purity and concentration was determined using the Nanodrop 2000 (Thermo  
 38 Fisher Scientific, Waltham, MA). RNA integrity was quantified using the 4200 TapeStation (Agilent  
 39 Technologies, Santa Clara, CA) or Fragment Analyzer Automated CE System (Advanced Analytical  
 40 Technologies, Ankeny, IA). Libraries were prepared using the NEBNext Ultra II Directional Library Prep Kit  
 41 following Ribosomal Depletion (mouse enteroid RNA) or PolyA enrichment (HCT116 RNA) at the Cornell  
 42 Transcriptional Regulation and Expression Facility (Cornell University, Ithaca, NY). Libraries were then  
 43 sequenced using the NextSeq500 platform (Illumina, San Diego, CA).

34

35 **Small RNA-seq Analysis.** Read quality was assessed using FastQC. Trimming, mapping and quantification  
 36 was performed using miRquant 2.0 as described in Kanke et al., (2016)<sup>34</sup>. In short, reads were trimmed using  
 37 Cutadapt. In short, reads were trimmed using Cutadapt, aligned to the genome using Bowtie and SHRiMP, and

aligned reads were quantified and normalized using DESeq2. Defining groups of miRNAs with similar patterns of expression across genotypes: Raw miRNA count matrices produced by miRquant were analyzed using a likelihood ratio-test from DESeq2. miRNA annotations in the 5000s are degradation products and removed from the analysis, and miRNAs with an adjusted p-value greater than 0.05 and baseMean expression less than 500 were discarded. An rlog transformation was applied to the raw counts and batch effects were removed using the limma function removeBatchEffects. Clusters of miRNAs with similar expression patterns were identified using the DESeq2 (v1.26.0) function degPatterns (minc = 5). Only clusters containing greater than five miRNAs were considered. Fold change heatmaps: Transformation and batch correction of miRNA expression and grouping of miRNAs is described above. Normalized expression of miRNAs for each mutant enteroid sample was subtracted from average WT expression and heatmaps were made using the R package pheatmap (v1.0.12).

**RNA-seq Analysis.** Read quality was assessed using FastQC. RNA-seq reads were aligned to either the mm10 genome release for mouse enteroids or the hg38 genome release for the human HCT116 cells using STAR (v2.7.9a). Quantification was performed with Salmon (v1.4.0) using the GENCODE release 25 annotations. Normalization and differential expression analyses were performed utilizing DESeq2 (v1.30.1). miRhub analysis was performed as described in Baran-Gale et al. (2013)<sup>52</sup>. Enrichr was used for KEGG pathway analysis as described in Chen et al. (2013)<sup>53</sup>.

**Quantitative PCR.** Total RNA from human colonoids was extracted using the Trizol LS RNA isolation method described above. Total RNA from HCT116 cells was extracted using the Total RNA Purification Kit (Norgen Biotek, Thorold, ON, Canada) according to manufacturer's instructions. Reverse-transcription for miRNA expression was performed using the Taqman MicroRNA Reverse Transcription Kit (ThermoFisher Scientific, Waltham, MA). Quantification of miRNA expression was done using the TaqMan Universal PCR Master Mix

(ThermoFisher Scientific, Waltham, MA). miRNA expression was normalized to U6 (assay ID: 001973) or RNU48 (assay ID: 001006). miRNA Taqman assays: miR-375-3p (assay ID: 000564), miR-24-3p (assay ID: 000402). Reverse-transcription for gene expression was performed using the High-Capacity RNA-to-cDNA kit (ThermoFisher Scientific, Waltham, MA). Quantification of gene expression was done using the TaqMan Gene Expression Master Mix (ThermoFisher Scientific, Waltham, MA). Gene expression was normalized to *RPS9* (assay ID: Hs02339424\_g1). Gene Taqman assays: *HMOX1* (assay ID: Hs01110250\_m1), *PRSS8* (assay ID: Hs00173606\_m1). Measurements were taken using the BioRad CFX96 Touch Real Time PCR Detection System (Bio-Rad Laboratories, Richmond, CA).

**The Cancer Genome Atlas (TCGA) Analysis.** Data Download: RNA-seq High Throughput Sequencing (HTSeq) counts files for 382 primary colon tumor and 39 solid normal tissue samples using the NIHGDCC Data Transfer Tool. Normalization and differential expression were identified using DESeq2. miRNA quantification files, that used mirbase21, for 371 primary colon tumor and 8 solid normal tissue samples were also downloaded using NIHGDCC Data Transfer Tool. TCGA small RNA-seq across cancer types: Small RNA sequencing expression data was downloaded from TCGA for 23 tumor types using the R package TCGA-assembler. Expression was reported as the reads per million mapped to miRNAs (RPMMM). Log2 fold change was calculated by dividing the tumor expression by the expression in non-tumor tissue followed by log2 transformation.

**Generation of genetically modified human colonoids.** Colonoids were generated according to the methods described in Crespo et al. (2017)<sup>29</sup>. In short, human embryonic stem cells (HUES8 cells) were transduced with a dox-inducible CRISPR/Cas9 system. One million cells were treated with 3μM CHIR99021 (CHIR, Stem-RD) and 100 ng/mL Activin A (AA, R&D systems) in RPMI (Cellgro) media for 3 days. On day 3, CHIR was removed, and cells were grown in RPMI+AA for an additional day to generate definitive endoderm. To

differentiate to hindgut endoderm, cells were treated with CHIR and fibroblast growth factor 4 (FGF4, Peprotech) in RPMI+B27 (Gibco) media for 4 days. Following, cells were treated with CHIR, 300 nM LDN193189 (LDN, Axon) + 500 ng/mL epidermal growth factor (EGF, R&D) in DMEM/F12 media (Invitrogen)+B27 for an additional 12 days to generate colonic epithelial cells. Cells were then dissociated and embedded in Matrigel beads (BD Biosciences) where single cells were allowed to expand and eventually form colonic organoids after 28 days. Afterwards, colonoids were treated with doxycycline every two days for one month before harvesting for total RNA isolation using the Total RNA Purification Kit (Norgen Biotek, Thorold, ON, Canada) according to manufacturer's instructions or Trizol LS method described above.

**Mouse enteroid culture.** Crypts from the jejunum of 3-5 month old male B62J mice were isolated as described in Peck et al., (2017)<sup>62</sup>. Isolated crypts were plated in Reduced Growth Factor Matrigel (Corning, Corning, NY, catalog #: 356231) on Day 0. Advanced DMEM/F12 (Gibco, Gaithersburg, MD, catalog #: 12634-028) was used for culture and supplemented with GlutaMAX (Gibco, Gaithersburg, MD, catalog #:35050-061), Pen/Strep (Gibco, Gaithersburg, MD, catalog #:15140), HEPES (Gibco, Gaithersburg, MD, catalog #:15630-080), N2 supplement (Gibco, Gaithersburg, MD, catalog #:17502-048), 50 ng/mL EGF (R&D Systems, Minneapolis, MN, catalog #: 2028-EG), 100 ug/mL Noggin (PeproTech, Rocky Hill, NJ, catalog #: 250-38), 250 ng/uL murine R-spondin (R&D Systems, catalog #: 3474-RS-050), and 10 mM Y27632 (Enzo Life Sciences, Farmingdale, NY, catalog #:ALX270-333-M025) miR-24-3p LNA inhibitor treatment. Cells were transfected with hsa-miR-24-3p miRCURY LNA miRNA Power Inhibitor (Qiagen, Germantown, MD, catalog #: YI04101706-DDA) or Power Negative Control A (Qiagen, Germantown, MD, catalog #: YI00199006-DDA) to a final concentration of 500 nM on Day 0 using gymosis. Media was changed and cells were treated with 250 nM miR-24 LNA inhibitor or scramble. Cells were harvested and fixed in 4% (v/v) paraformaldehyde on Day 5.

Tgf- $\beta$  treatment. Recombinant Human TGF- $\beta$ 1 (PeproTech catalog #: 100-21) was added to enteroid media on Day 0 for final concentration of 0, 0.5, or 1 ng/mL. Enteroids were harvested on Day 3.

70

71 **HCT116 Transfection:** HCT116 cells were plated in DMEM+10% FBS media at a density of 3400 cells/well  
 72 in a 96-well plate. Cells incubated for 24 hours in a 37 °C incubator. Cells were transfected with hsa-miR-24-3p  
 73 miRCURY LNA miRNA Power Inhibitor (Qiagen, Germantown, MD, catalog #: YI04101706-DDA) or  
 74 scramble control to a final concentration of 100 nM using Lipofectamine 3000 (ThermoFisher Scientific,  
 75 Waltham, MA, catalog #: L3000-008) according to manufacturer's instructions. Either Power Negative Control  
 76 A (Qiagen, Germantown, MD, catalog #: YI00199006-DDA) or Negative Control miRCURY LNA miRNA  
 77 Mimic (Qiagen, Germantown, MD, catalog #: YM00479902-AGA) was used for scramble control. After 24-  
 78 hours, media was replaced with complete media. Ferrostatin-1 treatment. At the time of LNA transfection, cells  
 79 were also treated with 0, 0.5, 2, 5, or 10 µM Ferrostatin-1 (Sigma-Aldrich, St. Louis, MO, catalog #: SML0583-  
 80 5MG). After 24-hours, media was replaced with complete media. Cells were harvested 48-hours post-  
 81 transfection.

82

83 **Cell count assay.** 48-hours following transfection, cells in 96-well plate were washed with PBS and treated  
 84 with 50 µL trypsin. Cells incubated for 5 minutes in 37 °C incubator. Cells were resuspended using 150 µL  
 85 complete media and transferred to clean 1.5 mL Eppendorf tubes. Cell concentration was calculated by adding  
 86 10 µL of cell suspension to chip for Biorad TC20 Automated Cell Counter (Bio-Rad Laboratories, Richmond,  
 87 CA).

88

89 **CellTiter-Glo assays.** 48-hours following transfection, cells in 96-well plate were incubated at room  
 90 temperature for 30 minutes. 100 µL of room temperature CellTiter-Glo reagent (Promega, Madison, WI) was  
 91 added to each well and placed on cell rocker for 2 minutes to lyse the cells. Afterwards, plate was incubated at  
 92 room temperature for 10 minutes. Luminescent signal was quantified using a Synergy 2 Microplate Reader  
 93 (Biotek, Winooski, VT; area scan; Integration = 0:00:50; Sensitivity = 135).

34

35 **EdU Assay.** 48-hours following transfection, cells in 96-well plate were incubated with 10  $\mu\text{mol/L}$  EdU at 37  
 36  $^{\circ}\text{C}$  in complete media for 1 hour. Cells were then fixed with 4% paraformaldehyde for 20 minutes at room  
 37 temperature and permeabilized using 0.5% Triton X-100 in PBS for 20 minutes. The Invitrogen Click-iT Plus  
 38 EdU AlexaFluor 488 Imaging Kit (Invitrogen, Waltham, MA, C10637) was used to detect EdU according to  
 39 manufacturer's instructions. Nuclei were stained using DAPI (ThermoFisher Scientific, Waltham, MA, catalog  
 40 #: D1306) and imaged using ZOE Fluorescent Cell Image (Bio-Rad Laboratories, Richmond, CA). Images were  
 41 analyzed using FIJI. For EdU positive cells, threshold value was set to 10. For analyzing particles, counted  
 42 those particles with size = 250-Infinity and circularity = 0.4-1.

33

44 **TUNEL Assay.** 48-hours following transfection, cells in 96-well plate were washed twice with PBS and fixed  
 45 using 4% paraformaldehyde for 15 minutes at room temperature. Permeabilization was performed by using  
 46 0.5% Triton X-100 in PBS for 20 minutes. Cells were washed twice with deionized water. Positive control wells  
 47 were treated with 1X DNase I, Amplification Grade (ThermoFisher Scientific, Waltham, MA, catalog #: 18068-  
 48 015) solution according to manufacturer's instructions. Labeling and detection of apoptotic cells was completed  
 49 using the Invitrogen Click-iT Plus TUNEL Assay for In Situ Apoptosis Detection 488 kit (Invitrogen, Waltham,  
 50 MA, catalog #: C10617) according to manufacturer's instructions. Nuclei were stained using DAPI  
 51 (ThermoFisher Scientific, Waltham, MA, catalog #: D1306) and imaged using ZOE Fluorescent Cell Image  
 52 (Bio-Rad Laboratories, Richmond, CA). Images were analyzed using FIJI. For TUNEL positive cells, threshold  
 53 value was set to 14. For analyzing particles, counted those particles with size = 250-Infinity and circularity =  
 54 0.4-1.

15

16 **LNA24 transfection with leChRO-seq and RNA-seq cross comparison.** HCT116 cells were plated in  
 17 DMEM+10% FBS media at a density of 102,000 cells/well in a 6-well plate. Cells incubated for 24 hours in a

37 °C incubator and transfected with hsa-miR-24-3p miRCURY LNA miRNA Power Inhibitor (Qiagen, Germantown, MD, catalog #: YI04101706-DDA) or Power Negative Control A (Qiagen, Germantown, MD, catalog #: YI00199006-DDA) to a final concentration of 100 nM using Lipofectamine 3000 (ThermoFisher Scientific, Waltham, MA, catalog #: L3000-008). After 24-hours, media was replaced with complete media. After 48-hours post-transfection, cells were resuspended using 0.25% Trypsin (ThermoFisher Scientific, Waltham, MA, catalog #: 25200-114). Wells from the same treatment condition were pooled together into a single tube during each experimental replicate. 20,000 cells were isolated for total RNA isolation using the Total RNA Purification Kit (Norgen Biotek, Thorold, ON, Canada) according to manufacturer's instructions. RNA-seq and quantitative qPCR were performed as described previously.

The remaining cells (450,000+ cells) were flash frozen using 100% EtOH and dry ice until utilized for Length Extension Chromatin Run-On Sequencing (leChRO-seq) as described in Chu et al., (2018)<sup>30</sup>. Chromatin Isolation. Chromatin was isolated by treating cell pellet with 750μL 1X NUN buffer (20 mM HEPES, 7.5 mM MgCl<sub>2</sub>, 0.2 mM EDTA, 0.3 M NaCl, 1 M Urea, 1% NP-40, 1mM DTT, and 50 units/mL RNase Cocktail Enzyme (ThermoFisher Scientific, Waltham, MA), and 1X 50X Protease Inhibitor Cocktail (Roche, Branchburg, NJ)). Samples were vortexed vigorously for 1 minute to physically lyse the samples. An additional 750μL of 1X NUN buffer was added and samples were vortexed again for 1 minute. Cell lysates were incubated in an Eppendorf Thermomixer (Eppendorf, Hamburg, Germany) at 12°C and shaken at 2000 rpm for 30 minutes. Chromatin was pelleted by centrifuging samples at 12,500 x g for 30 minutes at 4 °C. Supernatant was removed and chromatin was washed 3 times with 1 mL 50 mM Tris-HCl (pH=7.5) containing 40 units/mL SUPERase In RNase Inhibitor. After removing supernatant from final wash, 50 μL storage buffer was added to chromatin and samples were transferred to 1.5 mL Bioruptor Microtubes with Caps for Bioruptor (Diagenode, Denville, NJ). Samples were then loaded into Pico Biorupter (Diagenode, Denville, NJ) and sonicated on high for 10 cycles (1 cycle = 30 seconds on, 30 seconds off). Sonication was repeated until chromatin was solubilized (max 3 cycles). Samples were stored at -80 °C until further processing. ChRO-seq library



**preparation and sequencing.** 50  $\mu$ L of 2X Biotin-11 Reaction mix (10 mM Tris-HCl pH=8.0, 5 mM  $MgCl_2$ , 1 mM DTT, 300 mM KCl, 400  $\mu$ M ATP, 0.8  $\mu$ M CTP, 400  $\mu$ M GTP, 400  $\mu$ M UTP, 40  $\mu$ M Biotin-11-CTP (Perkin Elmer, Waltham, MA, NEL542001EA), 100 ng yeast tRNA (VWR, Radnor, PA, 80054-306), 0.8 units/ $\mu$ L SUPERase In RNase Inhibitor, 1% sarkosyl) was added to 50  $\mu$ L solubilized chromatin. Samples were placed in Eppendorf Thermomixer at 37°C for 5 minutes and shaken at 750 rpm. Run-on was halted by adding 300  $\mu$ L Trizol LS (Life Technologies, 10296-010) and allowing the samples to incubate at room temperature for 3 minutes. RNA was purified using streptavidin beads (New England Biolabs, Ipswich, MA, S1421S) and ethanol precipitated with the co-precipitate GlycoBlue (Ambion, AM9515). Ligation of the 3' adaptor was done using the T4 RNA Ligase 1 (New England Biolabs, Ipswich, MA, M0204L). Ligation of 5' adaptor required (i) Removal of the 5' cap using RNA 5' pyrophosphohydrolase (RppH, New England Biolabs, Ipswich, MA, M0356S) (ii) Phosphorylation of the 5' end using T4 polynucleotide kinase (New England Biolabs, Ipswich, MA, M0201L) (iii) 5' adaptor ligation using T4 RNA Ligase 1 (New England Biolabs, Ipswich, MA, M0204L). Generation of cDNA was done by using Superscript III Reverse Transcriptase (Life Technologies, 18080-044). Amplification was completed by using Q5 High-Fidelity DNA Polymerase (New England Biolabs, Ipswich, MA, M0491L). Single-end sequencing (5' end, 75 bp) was performed at the Cornell Biotechnology Research Center using the NextSeq500 (Illumina, San Diego, CA) platform. **Data analysis.** To prepare bigwig files for further analyses, leChRO-seq libraries were aligned to the hg38 genome using the proseq2.0 pipeline (<https://github.com/Danko-Lab/proseq2.0>) in single-end mode (Chu et al., 2018)<sup>30</sup>. Annotation of leChRO-seq reads excluded reads within 500 bp downstream of the transcription start site (TSS) to account for RNA polymerase pausing at the gene promoters. Genes <1000 bp were then excluded to account for the bias resulting from short gene bodies. ChRO-seq reads were normalized and differential expression analysis was performed using DESeq2.

**Statistics.** All statistical tests used are detailed in the figure legends. Either two-tailed Welch t-test (calculated using R) or two-tailed Student's t-test (calculated using excel) was applied to datasets that were normalized



(DESeq2, log2, rlog). Significance for data sets that did not statistically differ from a normal distribution (Shapiro-Wilk test p-value > 0.05) was calculated using a t-test. A two-sided Wilcoxon test was applied to non-parametric data sets unless where indicated. P-values < 0.05 are considered statistically significant. NS. = not significant, \* = p<0.05, \*\* = p<0.01, \*\*\* = p<0.001.

## Data availability

The datasets supporting the conclusions of this article are available in the Gene Expression Omnibus (GEO) repository, accession GSE188212 <https://www.ncbi.nlm.nih.gov/geo/query/acc.cgi?acc=GSE188212>. DESeq2 differential expression statistics are available at <https://jwvillan.shinyapps.io/ME-MIRAGE/>.

## References.

1. Sung, H. *et al.* Global Cancer Statistics 2020: GLOBOCAN Estimates of Incidence and Mortality Worldwide for 36 Cancers in 185 Countries. *Ca Cancer J Clin* **71**, 209–249 (2021).
2. Network, T. C. G. A. Comprehensive molecular characterization of human colon and rectal cancer. *Nature* **487**, 330–337 (2012).
3. Dienstmann, R. *et al.* The consensus molecular subtypes of colorectal cancer. *Nature Medicine* 1–13 (2015) doi:10.1038/nm.3967.
4. Molinari, C. *et al.* Heterogeneity in Colorectal Cancer: A Challenge for Personalized Medicine? *Int J Mol Sci* **19**, 3733 (2018).
5. Punt, C. J. A., Koopman, M. & Vermeulen, L. From tumour heterogeneity to advances in precision treatment of colorectal cancer. *Nature reviews. Clinical oncology* **14**, 235–246 (2017).

6. Roock, W. D. *et al.* Effects of KRAS, BRAF, NRAS, and PIK3CA mutations on the efficacy of cetuximab plus chemotherapy in chemotherapy-refractory metastatic colorectal cancer: a retrospective consortium analysis. *Lancet Oncol* **11**, 753–762 (2010).
7. Sen, M. *et al.* ARID1A facilitates KRAS signaling-regulated enhancer activity in an AP1-dependent manner in colorectal cancer cells. *Clin Epigenetics* **11**, 92 (2019).
8. Rahnamoun, H. *et al.* Mutant p53 shapes the enhancer landscape of cancer cells in response to chronic immune signaling. *Nature Communications* 1–14 (2017) doi:10.1038/s41467-017-01117-y.
9. Necela, B. M., Carr, J. M., Asmann, Y. W. & Thompson, E. A. Differential Expression of MicroRNAs in Tumors from Chronically Inflamed or Genetic (APCMin/+) Models of Colon Cancer. *Plos One* **6**, e18501 (2011).
10. Bailey, J. M. *et al.* p53 mutations cooperate with oncogenic Kras to promote adenocarcinoma from pancreatic ductal cells. *Oncogene* **35**, 4282–4288 (2016).
11. Trobridge, P. *et al.* TGF-beta receptor inactivation and mutant Kras induce intestinal neoplasms in mice via a beta-catenin-independent pathway. *Gastroenterology* **136**, 1680–8.e7 (2009).
12. Han, T. *et al.* Lineage reversion drives WNT independence in intestinal cancer. *Cancer discovery* CD-19-1536 (2020) doi:10.1158/2159-8290.cd-19-1536.
13. Rahnamoun, H. *et al.* Mutant p53 shapes the enhancer landscape of cancer cells in response to chronic immune signaling. *Nature Communications* 1–14 (2017)
14. Liu, F. *et al.* EGFR Mutation Promotes Glioblastoma through Epigenome and Transcription Factor Network Remodeling. *Molecular Cell* **60**, 307–318 (2015).
15. Ibrahim, H. & Lim, Y. C. KRAS-associated microRNAs in colorectal cancer. *Oncol Rev* **14**, 454 (2020).
16. Jones, M. F. & Lal, A. MicroRNAs, wild-type and mutant p53: More questions than answers. *Rna Biol* **9**, 781–791 (2014).
17. Brown, D., Rahman, M. & Nana-Sinkam, S. P. MicroRNAs in Respiratory Disease. A Clinician's Overview. *Ann Am Thorac Soc* **11**, 1277–1285 (2014).

18. Fridrichova, I. & Zmetakova, I. MicroRNAs Contribute to Breast Cancer Invasiveness. *Cells* **8**, 1361 (2019).
19. Hao, N.-B., He, Y.-F., Li, X.-Q., Wang, K. & Wang, R.-L. The role of miRNA and lncRNA in gastric cancer. *Oncotarget* **5**, 81572–81582 (2015).
20. Ma, L. *et al.* Therapeutic silencing of miR-10b inhibits metastasis in a mouse mammary tumor model. *Nat Biotechnol* **28**, 341–347 (2010).
21. Hanna, J., Hossain, G. S. & Kocerha, J. The Potential for microRNA Therapeutics and Clinical Research. *Frontiers Genetics* **10**, 478 (2019).
22. Seto, A. G. *et al.* Cobomarsen, an oligonucleotide inhibitor of miR-155, coordinately regulates multiple survival pathways to reduce cellular proliferation and survival in cutaneous T-cell lymphoma. *Brit J Haematol* **183**, 428–444 (2018).
23. Cojocneanu, R. *et al.* Plasma and Tissue Specific miRNA Expression Pattern and Functional Analysis Associated to Colorectal Cancer Patients. *Cancers* **12**, 843 (2020).
24. Falzone, L. *et al.* Integrated analysis of colorectal cancer microRNA datasets: identification of microRNAs associated with tumor development. *Aging Albany Ny* **10**, 1000–1014 (2018).
25. Bandrés, E. *et al.* Identification by Real-time PCR of 13 mature microRNAs differentially expressed in colorectal cancer and non-tumoral tissues. *Mol Cancer* **5**, 29–29 (2006).
26. To, K. K., Tong, C. W., Wu, M. & Cho, W. C. MicroRNAs in the prognosis and therapy of colorectal cancer: From bench to bedside. *World J Gastroentero* **24**, 2949–2973 (2018).
27. Network, T. C. G. A. Comprehensive molecular characterization of human colon and rectal cancer. *Nature* **487**, 330–337 (2012).
28. Berg, K. C. G. *et al.* Multi-omics of 34 colorectal cancer cell lines - a resource for biomedical studies. 1–16 (2017) doi:10.1186/s12943-017-0691-y.
29. Crespo, M. *et al.* Colonic organoids derived from human induced pluripotent stem cells for modeling colorectal cancer and drug testing. *Nature Medicine* **23**, 878–884 (2017).

30. Chu, T. *et al.* Chromatin run-on and sequencing maps the transcriptional regulatory landscape of glioblastoma multiforme. *Nature Genetics* **50**, 1553–1564 (2018).
31. Schatoff, E. M. *et al.* Distinct CRC-associated APC mutations dictate response to Tankyrase inhibition. *Cancer discovery* CD-19-0289 (2019) doi:10.1158/2159-8290.cd-19-0289.
32. Dow, L. E. *et al.* Apc Restoration Promotes Cellular Differentiation and Reestablishes Crypt Homeostasis in Colorectal Cancer. *Cell* **161**, 1539–1552 (2015).
33. Han, T. *et al.* R-Spondin chromosome rearrangements drive Wnt-dependent tumour initiation and maintenance in the intestine. *Nature Communications* **8**, 1–12 (2017).
34. Kanke, M., Baran-Gale, J., Villanueva, J. & Sethupathy, P. miRquant 2.0: an Expanded Tool for Accurate Annotation and Quantification of MicroRNAs and their isomiRs from Small RNA-Sequencing Data. *Journal of integrative bioinformatics* **13**, 307 (2016).
35. Pantano L (2021). *DEGreport: Report of DEG analysis*. R package version 1.28.0, <http://lpantano.github.io/DEGreport/>.
36. Lu, D. *et al.* MicroRNA-146a promote cell migration and invasion in human colorectal cancer via carboxypeptidase M/src-FAK pathway. *Oncotarget* **8**, 22674–22684 (2017).
37. Khorrami, S. *et al.* MicroRNA-146a induces immune suppression and drug-resistant colorectal cancer cells. *Tumor Biol* **39**, 1010428317698365 (2017).
38. Wu, Y. *et al.* MicroRNA-21 (Mir-21) Promotes Cell Growth and Invasion by Repressing Tumor Suppressor PTEN in Colorectal Cancer. *Cell Physiol Biochem* **43**, 945–958 (2017).
39. Yu, Y. *et al.* miR-21 and miR-145 cooperation in regulation of colon cancer stem cells. *Mol Cancer* **14**, 98 (2015).
40. Wang, Z., Wei, W. & Sarkar, F. H. miR-23a, a Critical Regulator of “migR”ation and Metastasis in Colorectal Cancer. *Cancer Discov* **2**, 489–491 (2012).
41. Jahid, S. *et al.* miR-23a Promotes the Transition from Indolent to Invasive Colorectal Cancer. *Cancer Discov* **2**, 540–553 (2012).

42. Kawaguchi, Y. *et al.* Mutation Status of RAS, TP53, and SMAD4 is Superior to Mutation Status of RAS Alone for Predicting Prognosis after Resection of Colorectal Liver Metastases. *Clin Cancer Res* **25**, 5843–5851 (2019).
43. Matano, M. *et al.* Modeling colorectal cancer using CRISPR-Cas9-mediated engineering of human intestinal organoids. *Nat Med* **21**, 256–262 (2015).
44. Xie, M. *et al.* MicroRNA-30a regulates cell proliferation and tumor growth of colorectal cancer by targeting CD73. *Bmc Cancer* **17**, 305 (2017).
45. Baraniskin, A. *et al.* MiR-30a-5p suppresses tumor growth in colon carcinoma by targeting DTL. *Carcinogenesis* **33**, 732–739 (2012).
46. Liang, Z. *et al.* MiR-141-3p inhibits cell proliferation, migration and invasion by targeting TRAF5 in colorectal cancer. *Biochem Bioph Res Co* **514**, 699–705 (2019).
47. Long, Z. H. *et al.* miR-141 Inhibits Proliferation and Migration of Colorectal Cancer SW480 Cells. *Anticancer Res* **37**, 4345–4352 (2017).
48. Dinh, T. A. *et al.* MicroRNA-375 Suppresses the Growth and Invasion of Fibrolamellar Carcinoma. *Cellular and molecular gastroenterology and hepatology* **7**, 803–817 (2019).
49. Kang, W. *et al.* miR-375 is involved in Hippo pathway by targeting YAP1/TEAD4-CTGF axis in gastric carcinogenesis. *Cell Death Dis* **9**, 92 (2018).
50. Alam, K. J. *et al.* MicroRNA 375 regulates proliferation and migration of colon cancer cells by suppressing the CTGF-EGFR signaling pathway. *International Journal of Cancer* **141**, 1614–1629 (2017).
51. Love, M. I., Huber, W. & Anders, S. Moderated estimation of fold change and dispersion for RNA-seq data with DESeq2. *Genome biology* **15**, 550 (2014).
52. Baran-Gale, J., Fannin, E. E., Kurtz, C. L. & Sethupathy, P. Beta cell 5'-shifted isomiRs are candidate regulatory hubs in type 2 diabetes. *PLOS ONE* **8**, e73240 (2013).
53. Chen, E. Y. *et al.* Enrichr: interactive and collaborative HTML5 gene list enrichment analysis tool. *Bmc Bioinformatics* **14**, 128–128 (2013).

54. Kuleshov, M. V. *et al.* Enrichr: a comprehensive gene set enrichment analysis web server 2016 update.  
*Nucleic Acids Res* **44**, W90–W97 (2016).
55. Xie, Z. *et al.* Gene Set Knowledge Discovery with Enrichr. *Curr Protoc* **1**, e90 (2021).
56. Sarma, S. N., Kim, Y.-J., Song, M. & Ryu, J.-C. Induction of apoptosis in human leukemia cells through the  
production of reactive oxygen species and activation of HMOX1 and Noxa by benzene, toluene, and o-  
xylene. *Toxicology* **280**, 109–117 (2011).
57. Kwon, M.-Y., Park, E., Lee, S.-J. & Chung, S. W. Heme oxygenase-1 accelerates erastin-induced  
ferroptotic cell death. *Oncotarget* **6**, 24393–24403 (2015).
58. Zhang, L. *et al.* PRSS8 is Downregulated and Suppresses Tumour Growth and Metastases in Hepatocellular  
Carcinoma. *Cell Physiol Biochem* **40**, 757–769 (2016).
59. Wu, L., Gong, Y., Yan, T. & Zhang, H. LINP1 promotes the progression of cervical cancer by scaffolding  
EZH2, LSD1, and DNMT1 to inhibit the expression of KLF2 and PRSS8. *Biochem Cell Biol* **98**, 591–599  
(2020).
60. Wei, R., Yang, Q *et al.* microRNA-375 inhibits colorectal cancer cells proliferation by downregulating  
JAK2/STAT3 and MAP3K8/ERK signaling pathways. 1–9 (2017).
61. He, X.-X. *et al.* MicroRNA-375 targets AEG-1 in hepatocellular carcinoma and suppresses liver cancer cell  
growth in vitro and in vivo. *Oncogene* **31**, 3357–3369 (2012).
62. Peck, B. C. E. *et al.* Functional Transcriptomics in Diverse Intestinal Epithelial Cell Types Reveals Robust  
MicroRNA Sensitivity in Intestinal Stem Cells to Microbial Status. *Journal of Biological Chemistry* **292**,  
2586–2600 (2017).
63. Mor, E. *et al.* Species-specific microRNA roles elucidated following astrocyte activation. *Nucleic Acids Res*  
**39**, 3710–3723 (2011).
64. Gao, Z. *et al.* miR-24-3p promotes colon cancer progression by targeting ING1. *Signal transduction and  
targeted therapy* **5**, 171–3 (2020).

65. Zhang, H.-W. *et al.* Cancer-associated fibroblast-derived exosomal microRNA-24-3p enhances colon cancer cell resistance to MTX by down-regulating CDX2/HEPH axis. *Journal of cellular and molecular medicine* (2021) doi:10.1111/jcmm.15765.
66. Gao, Y. *et al.* Down-regulation of miR-24-3p in colorectal cancer is associated with malignant behavior. *Medical oncology (Northwood, London, England)* **32**, 362–8 (2015).
67. Zhang, Q., Li, W., Liu, G. & Tang, W. MicroRNA-24 regulates the growth and chemosensitivity of the human colorectal cancer cells by targeting RNA-binding protein DND1. *Journal of B.U.ON. □: official journal of the Balkan Union of Oncology* **24**, 1476–1481 (2019).
68. Chhabra, R., Dubey, R. & Saini, N. Cooperative and individualistic functions of the microRNAs in the miR-23a~27a~24-2 cluster and its implication in human diseases. *Mol Cancer* **9**, 232–232 (2010).
69. ZHU, X.-F. *et al.* Knockdown of heme oxygenase-1 promotes apoptosis and autophagy and enhances the cytotoxicity of doxorubicin in breast cancer cells. *Oncol Lett* **10**, 2974–2980 (2015).
70. Petrache, I., Otterbein, L. E., Alam, J., Wiegand, G. W. & Choi, A. M. K. Heme oxygenase-1 inhibits TNF- $\alpha$ -induced apoptosis in cultured fibroblasts. *Am J Physiol-lung C* **278**, L312–L319 (2000).
71. Becker, J. C. *et al.* Colonic expression of heme oxygenase-1 is associated with a better long-term survival in patients with colorectal cancer. *Scand J Gastroentero* **42**, 852–858 (2009).
72. Ishikawa, T. *et al.* Different effects of constitutive nitric oxide synthase and heme oxygenase on pulmonary or liver metastasis of colon cancer in mice. *Clin Exp Metastas* **20**, 445–450 (2003).
73. Hofmans, S. *et al.* Novel Ferroptosis Inhibitors with Improved Potency and ADME Properties. *J Med Chem* **59**, 2041–2053 (2016).
74. Guo, J. *et al.* Ferroptosis: A Novel Anti-tumor Action for Cisplatin. *Cancer research and treatment □: official journal of Korean Cancer Association* **50**, 445–460 (2018).
75. Dienstmann, R. *et al.* The consensus molecular subtypes of colorectal cancer. *Nature Medicine* 1–13 (2015).
76. Jackson, E. L. *et al.* Analysis of lung tumor initiation and progression using conditional expression of oncogenic K-ras. *Gene Dev* **15**, 3243–3248 (2001).

39

## 40 **Author Contributions.**

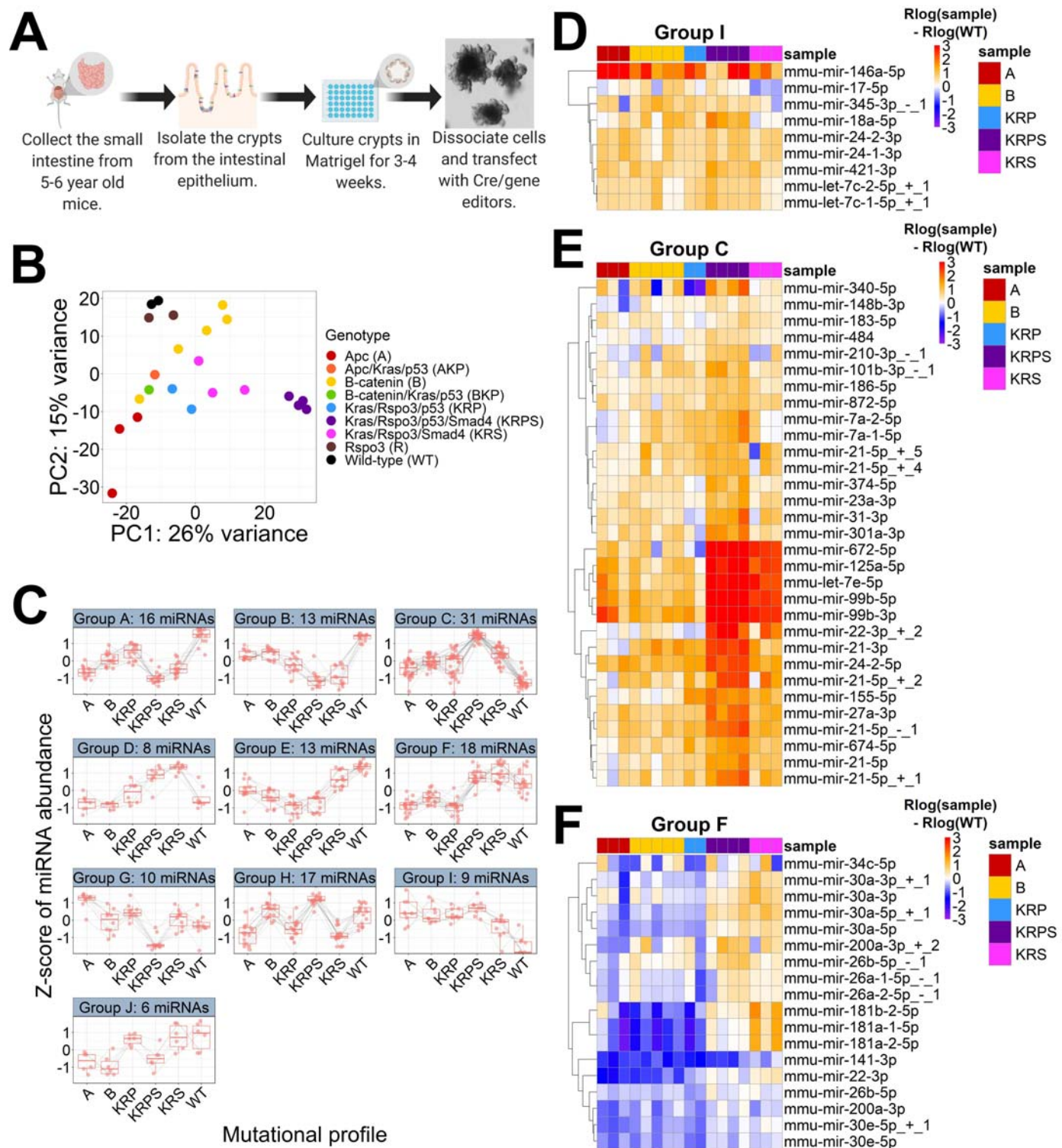
41 J.W.V, C.G.D, and P.S designed the research. L.K completed miR-24 inhibitor optimization and cellTiter-  
 42 glo/cell count analyses in HCT116 following miR-24 inhibition. T.H, S.A.M, and L.E.D generated and/or  
 43 expanded genetically modified mouse enteroid models. F.C.P and S.C generated and/or expanded genetically  
 44 modified human colonoid models. M.T.S cultured WT mouse enteroids for miR-24 inhibitor and Tgf- $\beta$   
 45 experiments. M.K downloaded and generated plot of miR-24 expression across TCGA tumor types. J.W.V  
 46 completed remaining wet lab experiments and computational analyses. J.W.V, C.G.D, and P.S wrote the paper.  
 47 All authors reviewed and approved the paper.

48

## 49 **Competing interests.**

50 The authors declare that they have no competing interests.





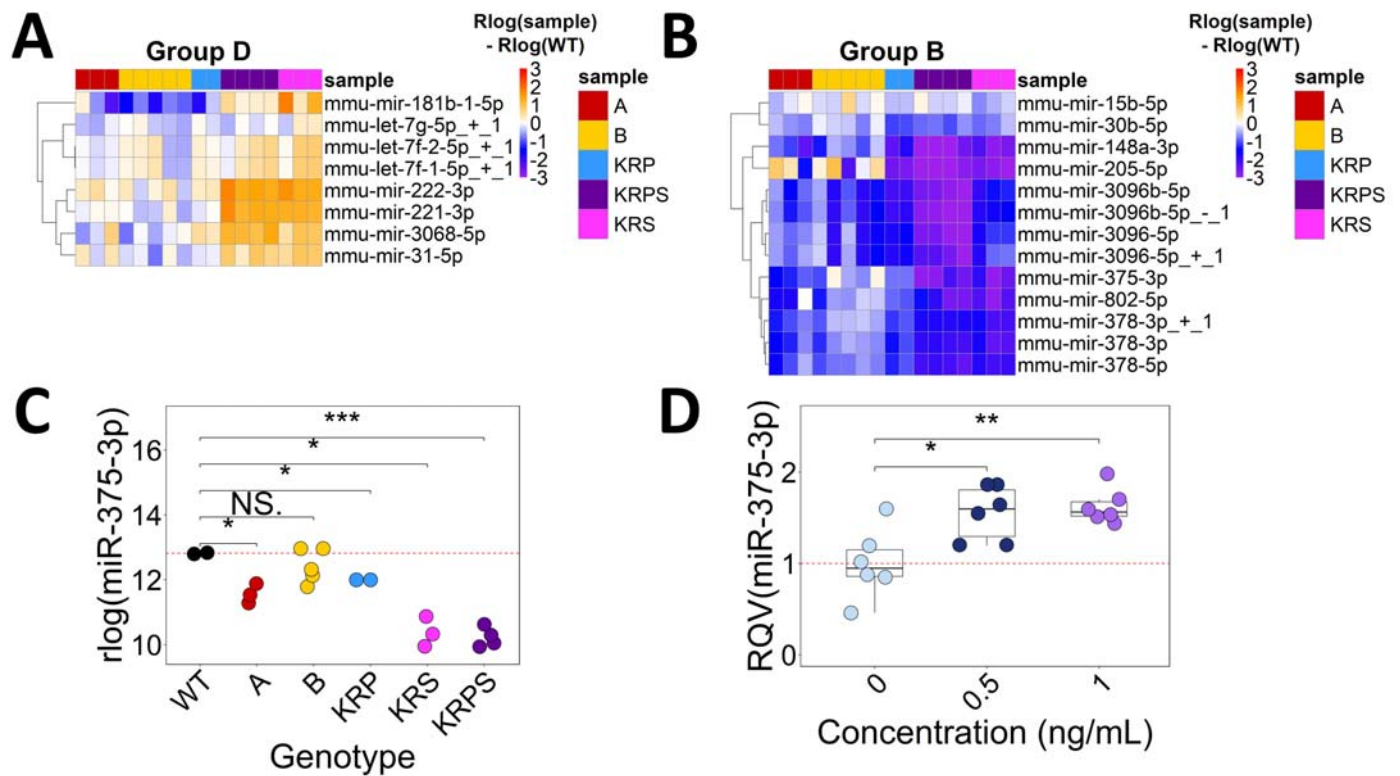
**Figure 1: Genetically modified enteroids exhibit mutation-dependent variation in miRNA expression.** (A)

Diagram illustrating how enteroid models were generated (Created with BioRender.com). (B) Principal

component analysis (PCA) plot generated using miRNA expression profiles from *Apc* (A; n=3), *Apc/Kras/p53*

(AKP; n=1), *B-catenin* (B; n=5), *B-catenin/Kras/p53* (BKP; n=1), *Kras/Rspo3/p53* (KRP; n=2),

*Kras/Rspo3/p53/Smad4* (KRPS; n=4), *Kras/Rspo3/Smad4* (KRS; n=3), *Rspo3* (R; n=2) mutant enteroids, and wild-type (WT; n=2) controls. (C) Z-score of miRNA abundance for the 10 modules of miRNA expression, each with greater than 5 miRNAs in the module, as defined by DEGReport. Only miRNAs with baseMean > 500 and p-adj < 0.05 following DESeq2 likelihood ratio test (LRT) are included in the analysis. (D-F) Heatmaps showing rlog normalized miRNA expression in each genetically modified enteroid sample subtracted from average WT for miRNAs assigned to Group I, Group E and Group F by DEGReport. Color intensity shows the difference between rlog normalized miRNA expression and average WT. Color scale minimum saturates at -3 and maximum saturates at 3.



**Figure 2: Smad4 signaling is a major driver of miR-375-3p expression in mouse enteroids. (A, B)**

Heatmaps showing rlog normalized miRNA expression in each genetically modified enteroid sample subtracted from average WT for miRNAs assigned to Group D and Group B by DEGReport. Color intensity shows rlog normalized miRNA expression in each genetically modified enteroid sample subtracted from average WT. Color scale minimum saturates at -3 and maximum saturates at 3. (C) Normalized miR-375-3p expression from small RNA-seq in each genotype. (D) MiR-375-3p expression from RT-qPCR following 0, 0.5, or 1 ng/mL treatment of mouse enteroids with recombinant human TGF- $\beta$ 1. Significance in (C) and (D) determined according to two-tailed Welch t-test. \* $p < 0.05$ , \*\* $p < 0.01$ , \*\*\* $p < 0.001$ .



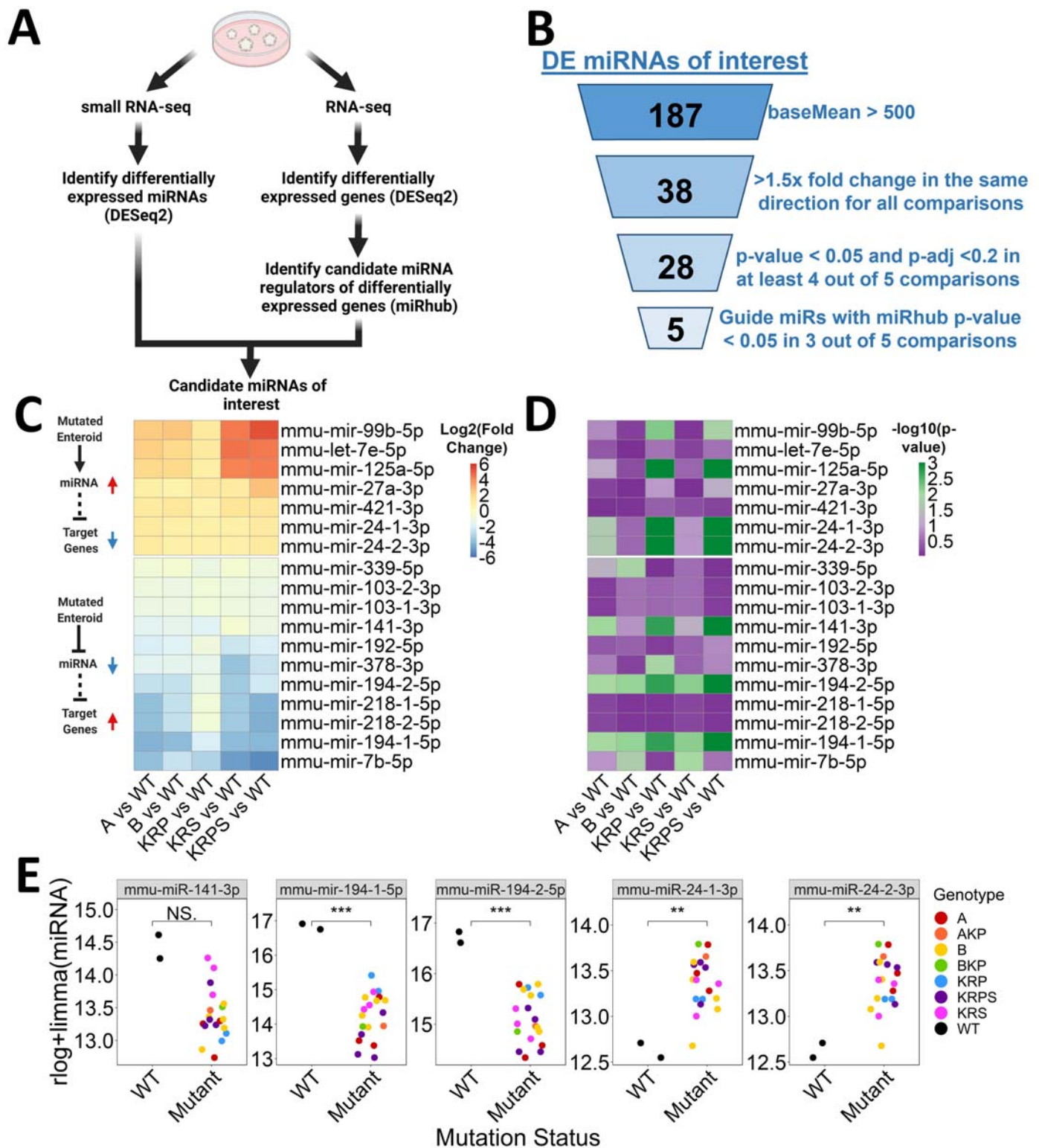


**Figure 3: Identification of five candidate miRNA master regulators in genetically modified mouse**

**enteroid models of CRC.** (A) Schematic (Created with BioRender.com) and (B) results of the strategy utilized to identify candidate miRNA master regulators. (C) Heatmap showing log2 fold change for guide miRNAs that

14 are significantly differentially expressed in the same direction (DESeq2 p-value <0.05, p-adj <0.2, baseMean  
15 >500, >1.5x fold change), in at least 4 out of five mutant enteroids compared to WT. Color intensity represents  
16 the log2 fold change relative to WT. (D) Heatmap showing -log10(p-value) of target site enrichment, calculated  
17 by miRhub (cons2) for each differentially expressed miRNA from (C), in the list of genes that are differentially  
18 expressed (DESeq2 p-adj < 0.05, baseMean>500, >1.5x fold change) in the opposite direction of the miRNA.  
19 (E) Normalized expression from small RNA-seq for the five candidate master miRNA regulators. Significance  
20 determined by two-tailed Welch t-test. \*p<0.05, \*\*p<0.01, \*\*\*p<0.001.

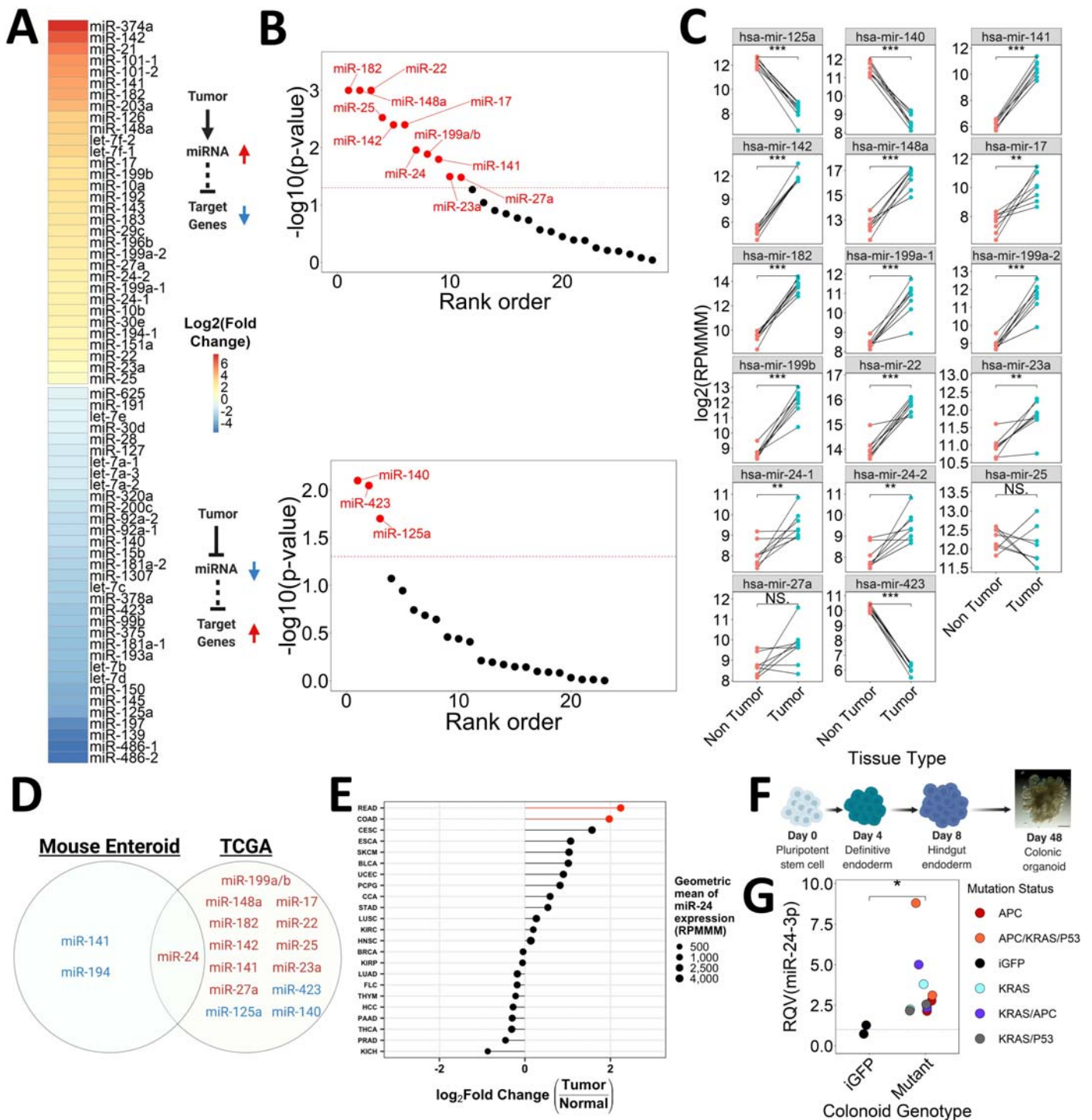


**Figure 4: miR-24-3p is a candidate master regulator of gene expression in the human colonic epithelium.**

(A) Heatmap showing the log<sub>2</sub> fold change for miRNAs differentially expressed (expression above 1000 reads per million mapped to miRNAs – RPMMM – in either condition, fold change >1.5x, p-adj<0.05) between TCGA primary colon adenocarcinoma (n=371) and non-tumor tissue (n=8). Color intensity represents the log<sub>2</sub>

fold change. (B) Plot of the  $-\log_{10}$  (p-value) of target site enrichment, calculated by miRhub (cons2) for each differentially expressed miRNA in (A), in the list of genes that are differentially expressed (DESeq2 expression above 1000 normalized counts in either condition, fold change  $>1.5x$ ,  $p\text{-adj}<0.05$ ) in the opposite direction of the miRNA. MiRNAs within the same family were grouped together under the same name (miR-24 and miR-199a/b). MiRNAs with target site enrichment  $p\text{-value}<0.05$  shown in red above the red dotted line. (C) Small RNA-seq counts ( $\log_2$  RPM) of the 17 miRNAs from (B) in matched TCGA primary colon adenocarcinoma ( $n=8$ ) and non-tumor ( $n=8$ ) tissue (two-tailed Welch t-test). Lines connect tissue samples collected from the same patient. (D) Venn diagram of the candidate master miRNA regulators of gene expression identified by the mouse enteroid and TCGA analyses (Created with BioRender.com). MiRNAs in red are upregulated. MiRNAs in blue are downregulated. Paralogs are listed as one miRNA. (E)  $\log_2$  fold change of miR-24-3p expression (RPM) across TCGA tumor types ( $n=23$ ). Colon (COAD) and rectal (READ) adenocarcinomas highlighted in red. Circle size represents the geometric mean (RPM) of miR-24-3p for each tumor type. (F) Diagram illustrating how human colonic organoid models were generated (Created with BioRender.com). (G) MiR-24-3p expression from RT-qPCR for mutant human colonic organoid models relative to inducible GFP (iGFP) control. Significance determined by two-sided Wilcoxon test.  $*p<0.05$ ,  $**p<0.01$ ,  $***p<0.001$ .



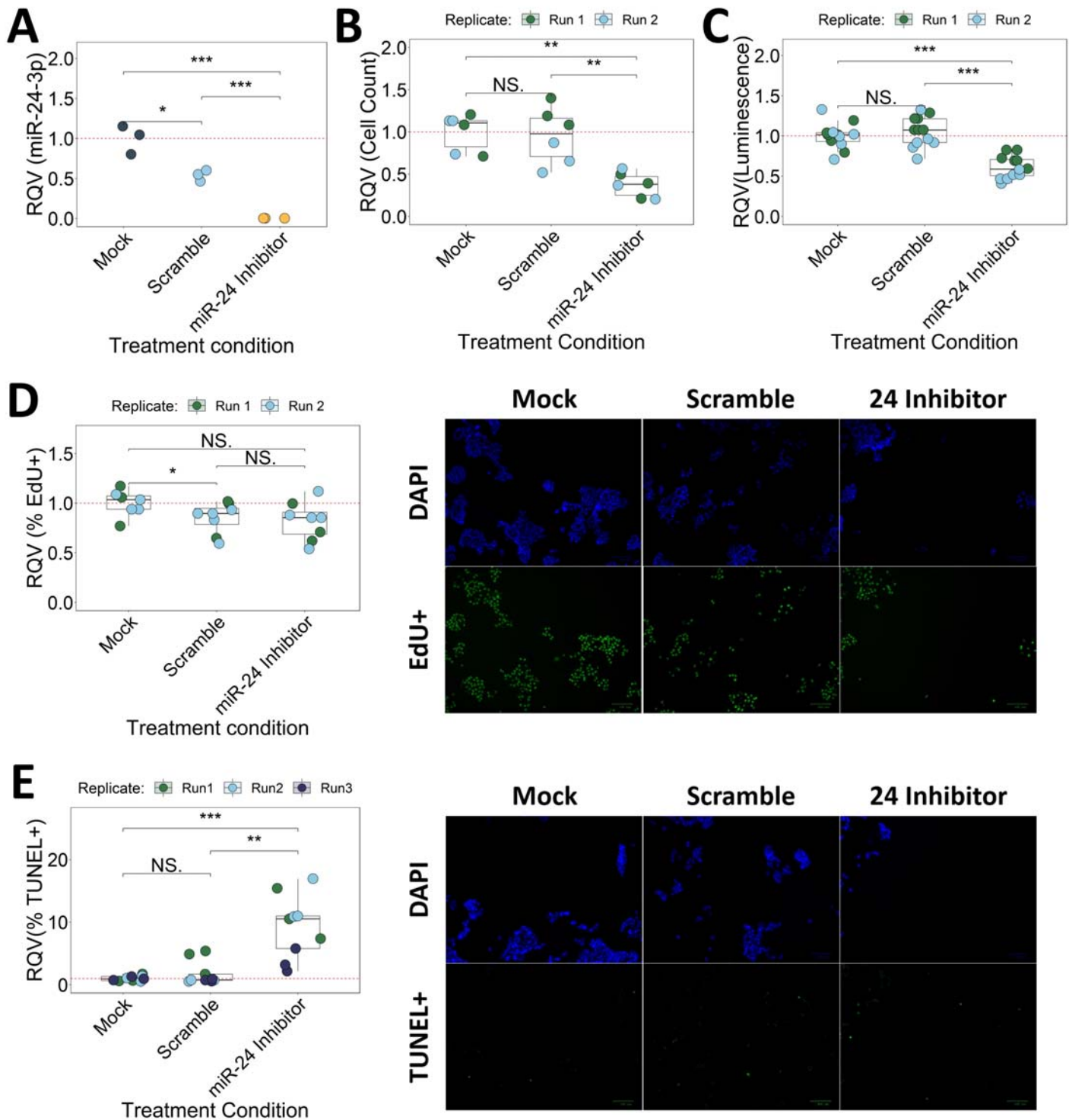


**Figure 5: Inhibition of miR-24-3p increases apoptosis in HCT116 cells.** (A) MiR-24-3p expression from RT-qPCR following mock, 100 nM scramble, or 100 nM miR-24 inhibitor treatment of HCT116 cells. Significance determined by two-tailed Student's t-test. Cell count (B), CellTiter-glo (C), EdU incorporation (D), and TUNEL (E) assays following mock, 100 nM scramble, or 100 nM miR-24 inhibitor treatment in HCT116



cells. Significance determined by two-sided Wilcoxon test. Results reported relative to average mock control. Color of data points represents experimental replicate. \* $p < 0.05$ , \*\* $p < 0.01$ , \*\*\* $p < 0.001$ .

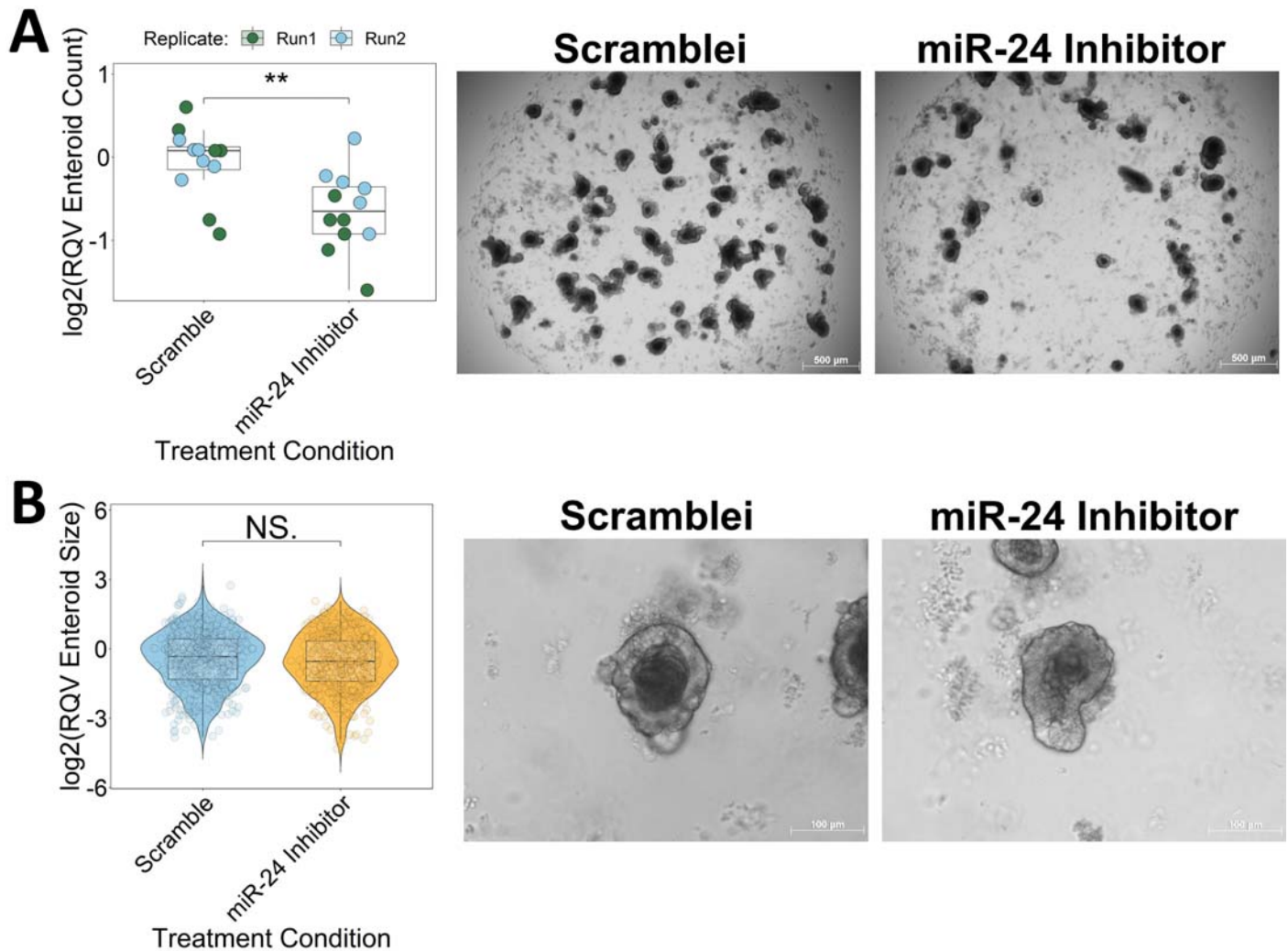


**Figure 6: miR-24-3p inhibition decreases mouse enteroid survival.** (A) Number of WT enteroids following scramble or miR-24 inhibitor treatment. Significance determined by two-tailed Welch t-test. Data reported relative to scramble average. Color of data points represents experimental replicate. (B) Violin plot of enteroid size across experimental replicates following scramble or miR-24 inhibitor treatment. Significance determined by two-tailed Welch t-test. Data reported relative to average scramble control. \* $p < 0.05$ , \*\* $p < 0.01$ , \*\*\* $p < 0.001$ .

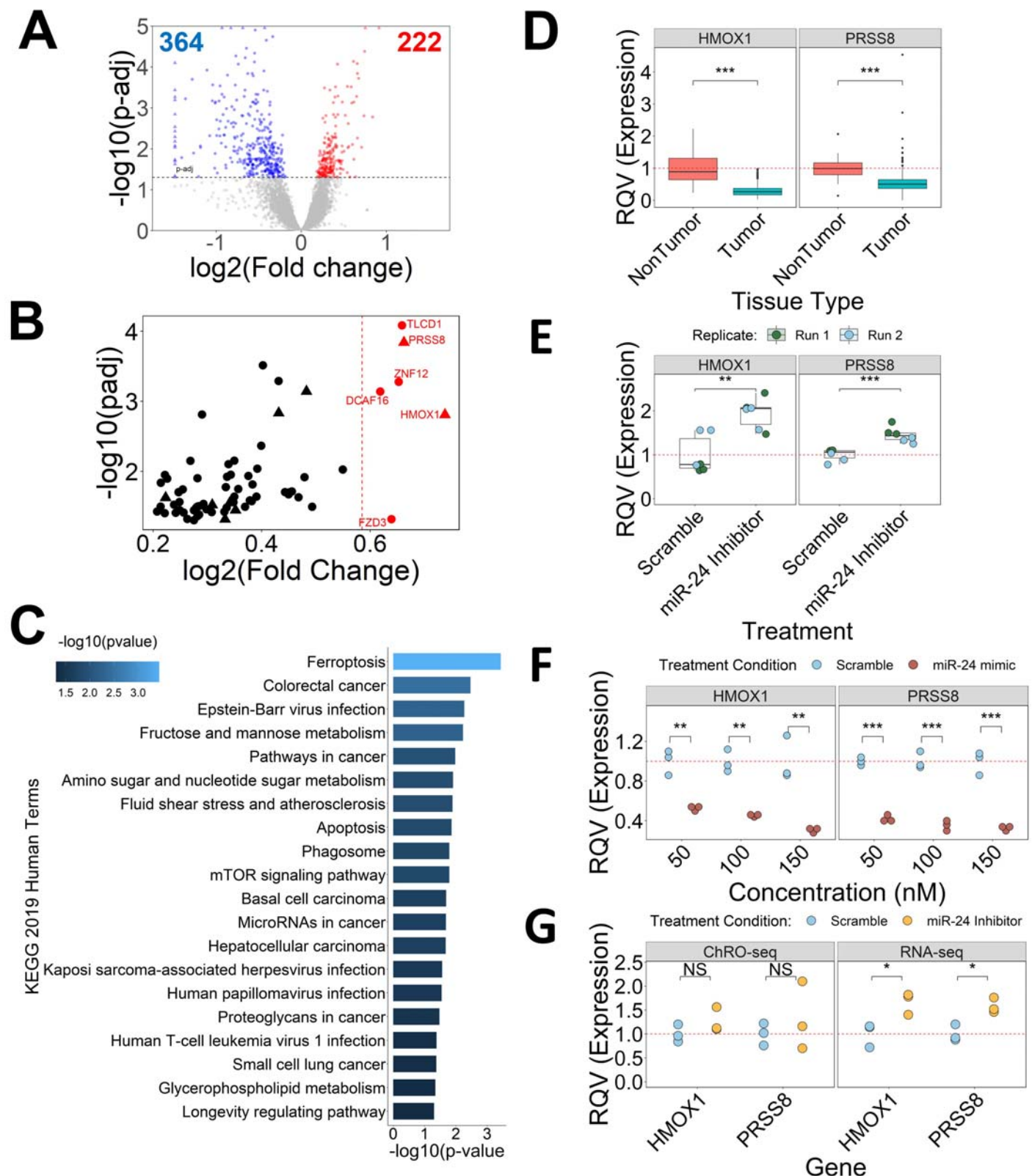


**Figure 7: HMOX1 is a direct target gene of miR-24 in the human colon context.** (A) Volcano plot showing differentially expressed genes in HCT116 treated with a 100 nM miR-24 inhibitor relative to scramble control.

Genes filtered for expression above 500 normalized counts in either condition. Horizontal dashed line represents p-adj cutoff of 0.05 (DESeq2). (B) Scatterplot of predicted miR-24-3p target genes that are upregulated (DESeq2 p-adj<0.05, >500 normalized counts in either condition) following miR-24-3p inhibition (n=70). Vertical red line represents 1.5x fold change. Genes in red exhibit >1.5x fold change (n=6). Genes that are also significantly downregulated in TCGA tumor tissue compared to non-tumor are represented by triangles. Remaining genes represented by circles. (C) KEGG pathway enrichment analysis of predicted miR-24-3p targets that are upregulated (n=70; DESeq2 p-adj<0.05, >500 normalized counts in either condition). Pathways with enrichment p-value <0.05 represented in figure. Color represents the -log<sub>10</sub> p-value. (D) Normalized expression from small RNA-seq of *HMOX1* and *PRSS8* in TCGA colon tumor relative to non-tumor tissue. Significance determined by two-tailed Welch t-test. (E) *HMOX1* and *PRSS8* expression from RT-qPCR following 100 nM scramble or miR-24 inhibitor treatment of HCT116 cells. Significance determined by two-tailed Welch t-test. Color of data points represents experimental replicate. (F) *HMOX1* and *PRSS8* expression from RT-qPCR following 50, 100 or 150 nM scramble or miR-24 mimic treatment of HCT116 cells. Significance determined by two-tailed Student's t-test. A non-parametric test was applied (two-sided Wilcoxon test), but significance was not achieved due to low sample size. (G) Relative expression from DESeq2 normalized *HMOX1* and *PRSS8* expression in HCT116 cells following 100 nM scramble or miR-24-inhibitor treatment. Significance determined by two-tailed Welch t-test. \*p<0.05, \*\*p<0.01, \*\*\*p<0.001.